# Centrosome and spindle assembly checkpoint loss leads to neural apoptosis and reduced brain size

John S. Poulton,[1,2] John C. Cuningham,[3] and Mark Peifer[1,3]

[1]Lineberger Comprehensive Cancer Center, [2]Department of Medicine, and [3]Department of Biology, University of North Carolina at Chapel Hill, Chapel Hill, NC 27599

Accurate mitotic spindle assembly is critical for mitotic fidelity and organismal development. Multiple processes coordinate spindle assembly and chromosome segregation. Two key components are centrosomes and the spindle assembly checkpoint (SAC), and mutations affecting either can cause human microcephaly. In vivo studies in *Drosophila melanogaster* found that loss of either component alone is well tolerated in the developing brain, in contrast to epithelial tissues of the imaginal discs. In this study, we reveal that one reason for that tolerance is the compensatory relationship between centrosomes and the SAC. In the absence of both centrosomes and the SAC, brain cells, including neural stem cells, experience massive errors in mitosis, leading to increased cell death, which reduces the neural progenitor pool and severely disrupts brain development. However, our data also demonstrate that neural cells are much more tolerant of aneuploidy than epithelial cells. Our data provide novel insights into the mechanisms by which different tissues manage genome stability and parallels with human microcephaly.

## Introduction

During cell division, proper mitotic spindle assembly ensures the replicated genome is equally partitioned into daughter cells via chromosome segregation. In animals, centrosomes and the spindle assembly checkpoint (SAC) regulate efficient and accurate mitotic spindle assembly. Centrosomes are the primary microtubule (MT)-organizing centers of the spindle. Although spindle assembly can occur in their absence, it is inefficient, and accuracy of chromosome segregation is generally compromised (Lerit and Poulton, 2016). The SAC restrains anaphase onset until all kinetochores are attached to MTs (Musacchio, 2015). Mutations in centrosomal and SAC genes can cause human disease, including primary microcephaly, mosaic variegated aneuploidy, and microcephalic primordial dwarfism (Klingseisen and Jackson, 2011; Megraw et al., 2011; Genin et al., 2012; Mirzaa et al., 2014; Nigg et al., 2014). Mechanisms by which the mutation of these genes leads to disease are a key question for the field.

Our earlier work in the epithelial cells of *Drosophila melanogaster* larval wing discs revealed that centrosome loss (*sas-4* mutant) leads to slowed spindle assembly, chromosome missegregation, and cell death (Poulton et al., 2014). In contrast, centrosome loss in larval fly brains does not elevate cell death (Basto et al., 2006) or cause microcephaly, but instead leads to brain tumors (Castellanos et al., 2008). Furthermore, although aneuploidy/polyploidy triggers apoptosis in imaginal discs (Dekanty et al., 2012; Poulton et al., 2014), mutations in mitotic regulators (e.g., Polo kinase, Asp, Separase, Grip91, and Sticky) lead to highly aneuploid and polyploid larval brain cells that continue to divide (Ripoll et al., 1985; Sunkel and Glover, 1988; Gatti and Baker, 1989). This suggests that these two tissues evolved different mechanisms to ensure mitotic fidelity or respond to mitotic errors. In wing imaginal discs, the SAC partially compensates for centrosome loss; discs depleted of both centrosomes and the SAC (*mad2 sas-4* double mutants) suffer massive cell death, leading to a complete loss of imaginal discs (Poulton et al., 2014). Given the apparent differences in how brain and wing disc cells respond to centrosome loss, we explored the roles of the SAC and centrosomes in the brain. We found that *mad2 sas-4* double mutant brains are dramatically smaller and highly disorganized, exhibiting increased apoptosis and chromosome missegregation. We also explored the mechanisms by which loss of centrosomes and the SAC leads to small brain size. These data shed light on the basis for the different responses to centrosome loss in imaginal disc epithelia versus neural stem cells.

## Results and discussion

### Combined loss of centrosomes and Mad2 leads to apoptosis and reduced brain size

Centrosome loss is well tolerated in larval brains. Based on our findings in wing discs, we hypothesized that the SAC compensates for centrosome loss in the brain. To test this, we compared

Correspondence to Mark Peifer: peifer@unc.edu; or John S. Poulton: poultonj@email.unc.edu

Abbreviations used: AEL, after egg laying; CB, central brain; MT, microtubule; NB, neuroblast; NEB, nuclear envelope breakdown; OOA, outer optic anlagen; SAC, spindle assembly checkpoint; WT, wild type.



The Rockefeller University Press $30.00
J. Cell Biol. Vol. 216 No. 5 1255–1265
https://doi.org/10.1083/jcb.201607022

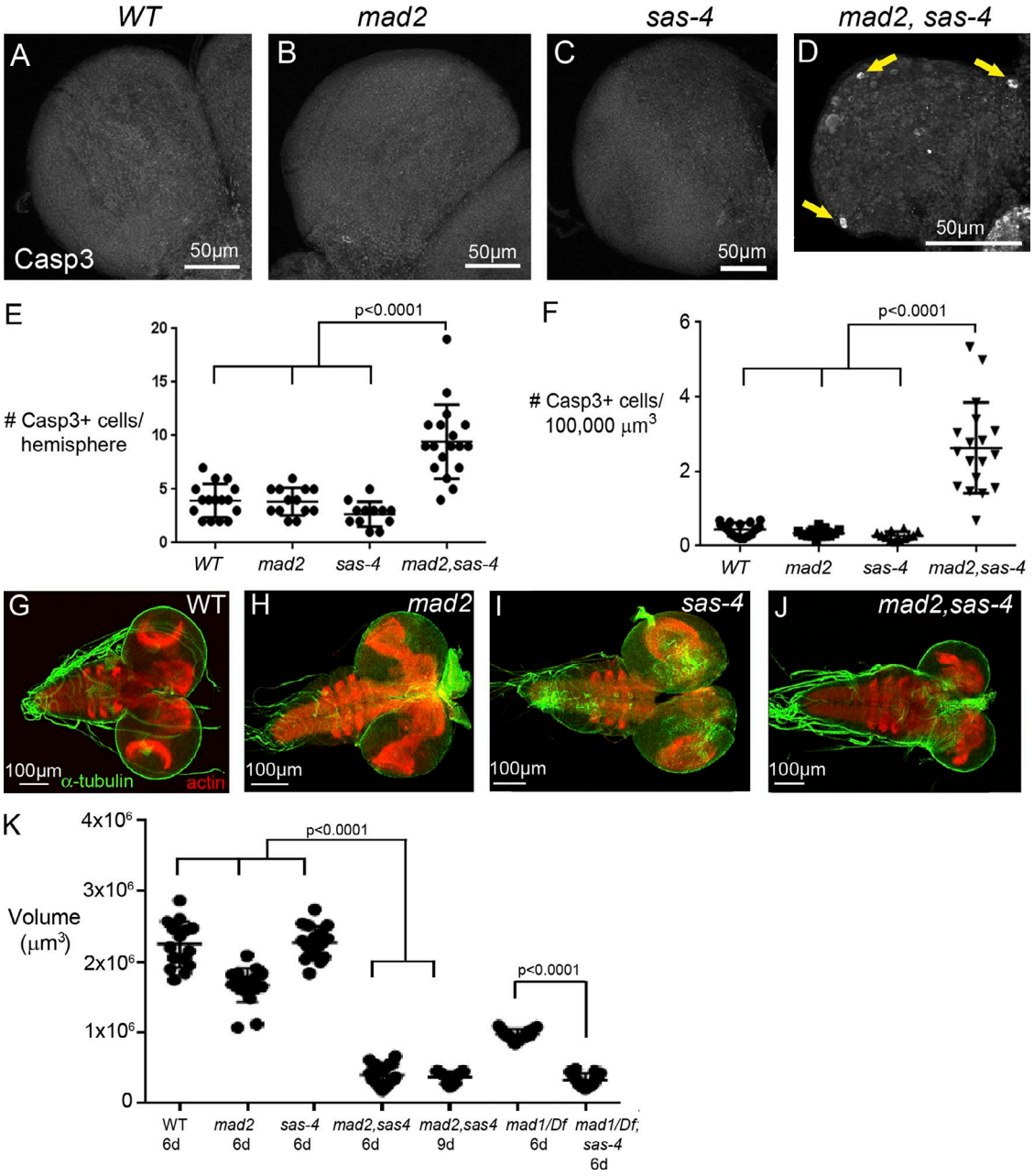


Figure 1. **Centrosomes and the SAC cooperate to promote neural stem cell viability and brain size.** (A–D) Apoptosis (cleaved Casp3) was not observed in WT (A), *mad2* (B), or *sas-4* single mutant brains (C), but *mad2 sas-4* double mutants displayed increased apoptosis (D). Arrows indicate apoptotic cells. (E and F) Samples were quantified per brain hemisphere (E) or standardized to brain size (F). (G–J) Third instar brains of indicated genotypes stained for actin (red) and α-tubulin (green). Note the smaller brains in *mad2 sas-4* double mutants as well as reduced optic lobes (see Fig. 2). (K) Brain size quantification. Both *mad2 sas-4* and *mad1/Df;sas-4* double mutant brains were significantly smaller than WT or the respective single mutants. *mad2* and *mad1* single mutant brains were also slightly smaller than WT or *sas-4* brains. Error bars represent means ± SD.

apoptosis (via cleaved Casp3 levels) in wild-type (WT) brains, single mutants lacking either centrosomes (*sas-4*) or the SAC (*mad2*), and double mutant brains (*mad2 sas-4*) from wandering third instar larvae (6 d after egg laying [AEL]). Although loss of centrosomes or the SAC alone did not elevate apoptosis in the brain (Buffin et al., 2007), *mad2 sas-4* mutant brains showed highly elevated apoptosis (Fig. 1, A–E). Because double mutant brains were much smaller than WT or single mutants (see next paragraph), cell death was even more pronounced when standardized for brain size (Fig. 1 F). The apoptosis markers Hid>GFP and cleaved Dcp-1 were similarly elevated (Fig. S1, A–H). These data suggest the SAC helps compensate for centrosome loss and prevent apoptosis.

We next examined how combined centrosome–SAC loss affects brain development. Although *mad2* or *sas-4* single mutants survived to adulthood (Basto et al., 2006; Buffin et al., 2007), double mutants arrested and died at the larval–pupal transition. Consistent with earlier work, third instar brains lacking just the SAC or centrosomes are similar in size to WT (Fig. 1, G–K; Basto et al., 2006; Buffin et al., 2007), though *mad2* brains were slightly smaller. However, brains lacking both centrosomes and the SAC were dramatically smaller than

WT or single mutants (Fig. 1, G–K; Caous et al., 2015). Similar results were seen with double mutants lacking the SAC and either of two key centrosomal proteins, asl or cnn (Fig. S1 I), as well as for *cnn* with *mad2* over a *mad2* deficiency (not depicted). To determine whether reduced brain size was caused by loss of the SAC or perhaps by a SAC-independent role of Mad2, we also examined animals lacking centrosomes plus Mad1, a different SAC component. Although *mad1/Df* single mutants were slightly smaller than WT, *mad1/Df*;*sas-4* double mutants were much smaller, on par with *mad2 sas-4* double mutants (Figs. 1 K and S1, J and K), suggesting that the reduced brain size we observed is caused by a combined loss of centrosomes and the SAC.

*mad2 sas-4* animals, like *sas-4* animals, are developmentally delayed (Poulton et al., 2014; unpublished data). We therefore considered whether the small brain size reflected a lack of sufficient time to grow to normal size. However, even at 9 d AEL, *mad2 sas-4* larval brains were still much smaller than day 6 WT or single mutants (Fig. 1 K). Thus, the combined activity of centrosomes and the SAC are required for normal brain size.

### Combined loss of centrosomes and the SAC leads to dramatic reduction in the optic lobes and disorganized brain architecture

To further characterize effects of centrosome plus SAC loss on brain development, we examined third instar brains. The fly brain becomes increasingly complex during larval development. Brain hemispheres develop distinct domains, with one demarcation being the separation of the central brain (CB) and optic lobe (Fig. 2 A). The WT CB contains ∼100 large neural stem cells called CB neuroblasts (NBs; Fig. 2, A and B; Urbach and Technau, 2003), which express the markers Deadpan (Dpn) and Miranda (Mira). NBs divide asymmetrically to maintain NB fate and generate distinct neuronal lineages via differentiating progeny (Homem and Knoblich, 2012). The WT optic lobe includes the horseshoe-shaped medulla and lamina, each with a band of neuroepithelial cells and many small NBs expressing Mira and Dpn (Fig. 2, A, B, E, and H). Loss of centrosomes or the SAC alone did not result in any obvious disruption of this architecture. Single mutant brains had a normal demarcation of the medulla from the CB, whether viewed from the anterior (Fig. 2, C and D vs. B) or posterior surfaces (on the posterior surface, apparently normal inner proliferative centers were visible; Fig. 2, F and G vs. E). In cross sections, each single mutant also had an apparently normal lamina (Fig. 2, I and J vs. H).

In contrast, organization of *mad2 sas-4* brains was substantially disrupted. Most notable was a loss or substantial reduction of the medulla—when viewed from either the anterior (Fig. 2, K and M vs. B) or posterior (Fig. 2, L vs. E), all that was seen in double mutants were disorganized regions of Mira/Dpn-expressing medullar NBs (Fig. 2, K–M). Cross-sectional views also did not reveal an obvious lamina in double mutants (not depicted). Visualizing WT third instar brains with phalloidin to stain F-actin also highlighted the medulla, including the more distal neuroepithelial cells, whose progeny will differentiate to become the medullar NBs (surface view, Fig. 2 N; cross section, Fig. 2, P and S). Single mutants appeared unaffected (Fig. S2, A and B, vs. Fig. 2 P). F-actin staining further substantiated the loss/disorganization of the medulla in double mutants (Fig. 2 O), though in cross sections, residual neuroepithelial cells were evident (Fig. 2, Q and T). E-cadherin (Ecad) staining revealed similar reduction/disorganization of the neuroepithelial cells in *mad2 sas-4* brains (Fig. S2, C vs. D). In WT, neuronal progeny of medullar NBs sent fasciculated axons in parallel bundles projecting into the medullar neuropil (Fig. 2, P and S; Hayden et al., 2007). These structures were unaffected in the single *mad2* or *sas-4* mutants (Fig. S2, E–H). Consistent with the reduction in medullar NBs, however, the medullar neuropil was strongly reduced in *mad2 sas-4* brains, and medullar axons were reduced and disorganized (Fig. 2, Q, R, and T). Similar severe defects in development of the medulla were also observed in *mad1/Df*;*sas-4* double mutants, with a loss or substantial reduction of the Dpn-positive medullar NBs, whereas *mad1/Df* single mutants resembled WT (Fig. S3, A–E).

The CB of WT, *mad2*, and *sas-4* single mutants appeared similar, with Mira/Dpn-positive CB NBs on both the anterior and posterior surfaces (Fig. 2, B–G). *mad2 sas-4* brains retained some discernable Mira/Dpn-positive CB NBs (Fig. 2, K and L), but some were highly enlarged (Fig. 2, K–M). *mad1/Df*;*sas-4* double mutants were similarly altered, retaining discernable though disorganized Dpn-positive CB NBs (Fig. S3 E). The neuronal progeny of many CB NBs remained associated with one another and sent bundled axons labeled with Ecad to targets in the CB (Fig. S2 I); similar structures were occasionally observed in *mad2 sas-4* brains (Fig. S2 J). A subset of CB NBs, the mushroom body NBs, never exited mitosis during earlier larval stages (Ito and Awasaki, 2008). By the third instar stage, their neuronal progeny had already created a structure known as the mushroom body, which can be visualized with the adhesion protein Fasciclin II (FasII; Fig. 2 U). This structure was present in single mutants (Fig. S2, K and L) and was also retained in *mad2 sas-4* brains (Fig. 2 V). *mad2 sas-4* brains lacked the network of FasII-positive axons that enter the medulla from the photoreceptors in the eye imaginal disc, but this was not surprising because double mutants lack imaginal discs (Poulton et al., 2014). Thus, although loss of centrosomes or the SAC is tolerated in developing brains, codepleting these mitotic regulators dramatically disrupts brain development.

### Combined loss of centrosomes and the SAC reduces both NB number and cell proliferation

In mammalian microcephaly, the cause of reduced brain size remains speculative. To determine whether the reduced size of *mad2 sas-4* brains reflected loss of neural progenitors, we quantified the CB NB number. Consistent with a recent study (Caous et al., 2015), *mad2 sas-4* brains had significantly fewer CB NBs, whether this was calculated per brain hemisphere (Fig. 3 B) or by area to account for reduced brain size (Fig. 3 C). It is also worth noting that centrosome loss alone increased NB number as a result of occasional symmetric NB divisions as was previously observed (Fig. 3 B; Rusan and Peifer, 2007; Cabernard and Doe, 2009; Wang et al., 2011). To determine whether CB NBs were among the apoptotic cells observed, we costained with Dpn and Casp3 (Fig. 3 D). In *mad2 sas-4* mutants, 24% of Casp3$^+$ cells also expressed Dpn ($n$ = 13/55; $n$ = five brains), and 5.4% of all Dpn$^+$ NBs were also Casp3$^+$ ($n$ = 13/240; $n$ = five brains). This suggests that cell death is an important contributor to the reduced NB pool and brain size in *mad2 sas-4* brains. To further test this, we blocked cell death by misexpressing the antiapoptotic protein p35 in *mad2 sas-4* brains. Consistent with a role for cell death in small brain size, p35 expression

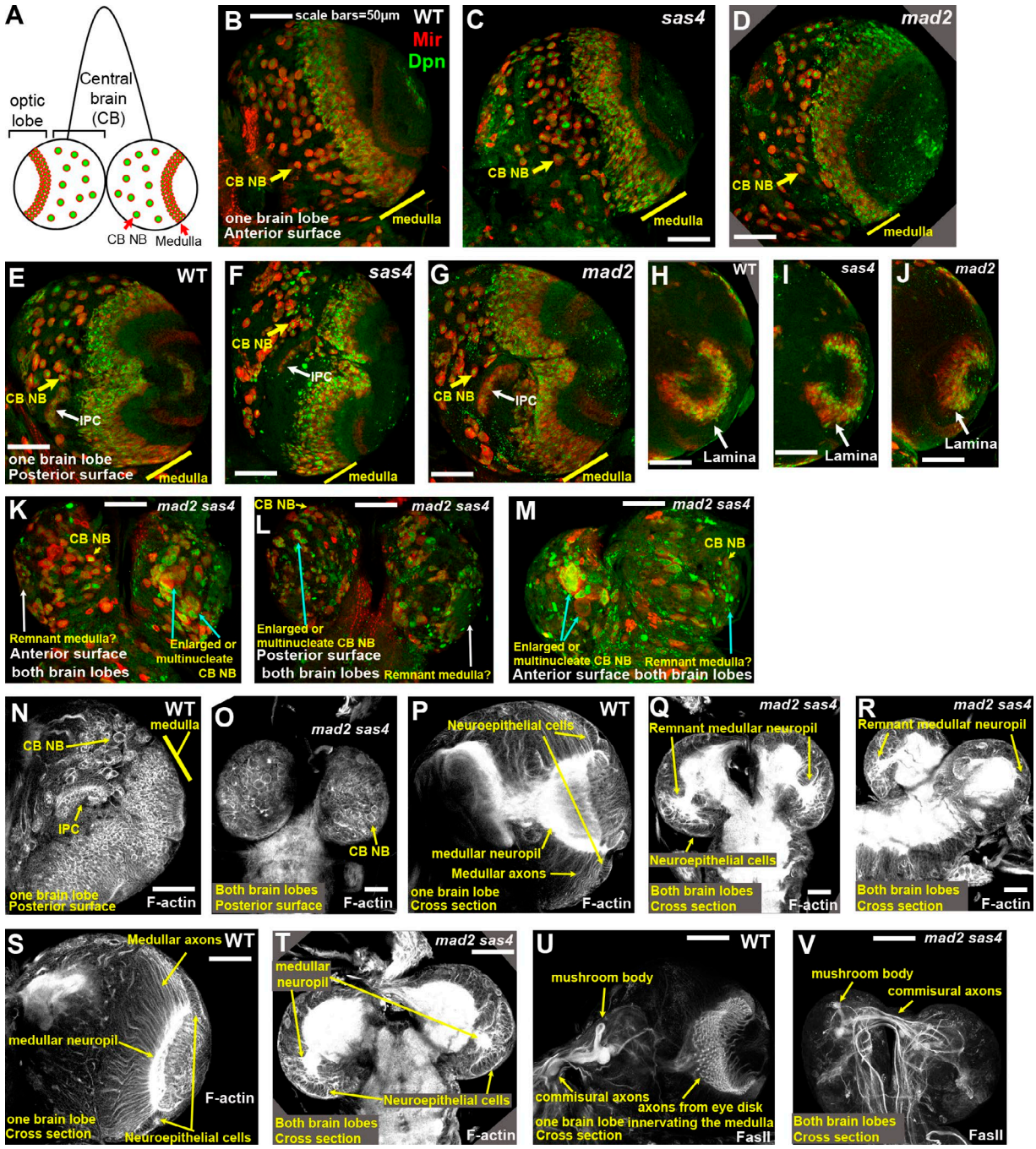


Figure 2. **Loss of centrosomes and the SAC dramatically alters brain architecture.** (A) Diagram of the third instar brain. Each hemisphere has an optic lobe and CB region containing many NBs (green and red circles). NBs expressed Dpn (green) and Mira (red). (B–M) WT, single, and double mutant brains stained for Dpn and Mira. (B–G) The horseshoe-shaped stripe of medulla NBs in WT (B and E) was also present in single mutants (C, D, F, and G), as was a normal lamina (H vs. I and J). Both were absent in *mad2 sas-4* (K–M), though residual medullar NBs may have remained. WT and single mutant CB NB populations were similar (B–G, yellow arrows). In double mutants, some seemingly normal CB NBs remained (K–M, yellow arrows), though others were very enlarged (K–M, blue arrows). (N–T) WT and double mutants labeled with F-actin (phalloidin). F-actin labeling also revealed substantial medulla reduction and retention of CB NBs in double mutants (N vs. O) as well as reduction/disorganization of medullar axons and the medullar neuropil (P and S vs. Q, R, and T), though some neuroepithelial cells remained in double mutants (Q and T). (U and V) WT and double mutant brains labeled with FasII. Double mutants retained a mushroom body and commissural axons but lacked incoming axons from eye disc photoreceptors. IPC, inner proliferative center.

significantly increased brain size in *mad2 sas-4* brains (Fig. 3, E–G), whereas p35 expression did not increase WT brain size (mean volume of p35 in WT = $1.3 \times 10^6$ μm$^3$; $n = 14$). We hypothesized that a reduced NB number in *mad2 sas-4* brains would also reduce the number of proliferating cells. Indeed, this was dramatically reduced relative to WT or single mutants (Fig. 4, A–E; and Videos 1 and 2; Caous et al., 2015). Other mechanisms may also contribute to reduced mitotic index, e.g., a prolonged cell cycle or premature differentiation (Gogendeau et al., 2015). Consistent with the latter, we observed a modest but significant increase in inappropriate NB differentiation (CB NBs expressing both Dpn and nuclear Prospero (Pros; Fig. S4,

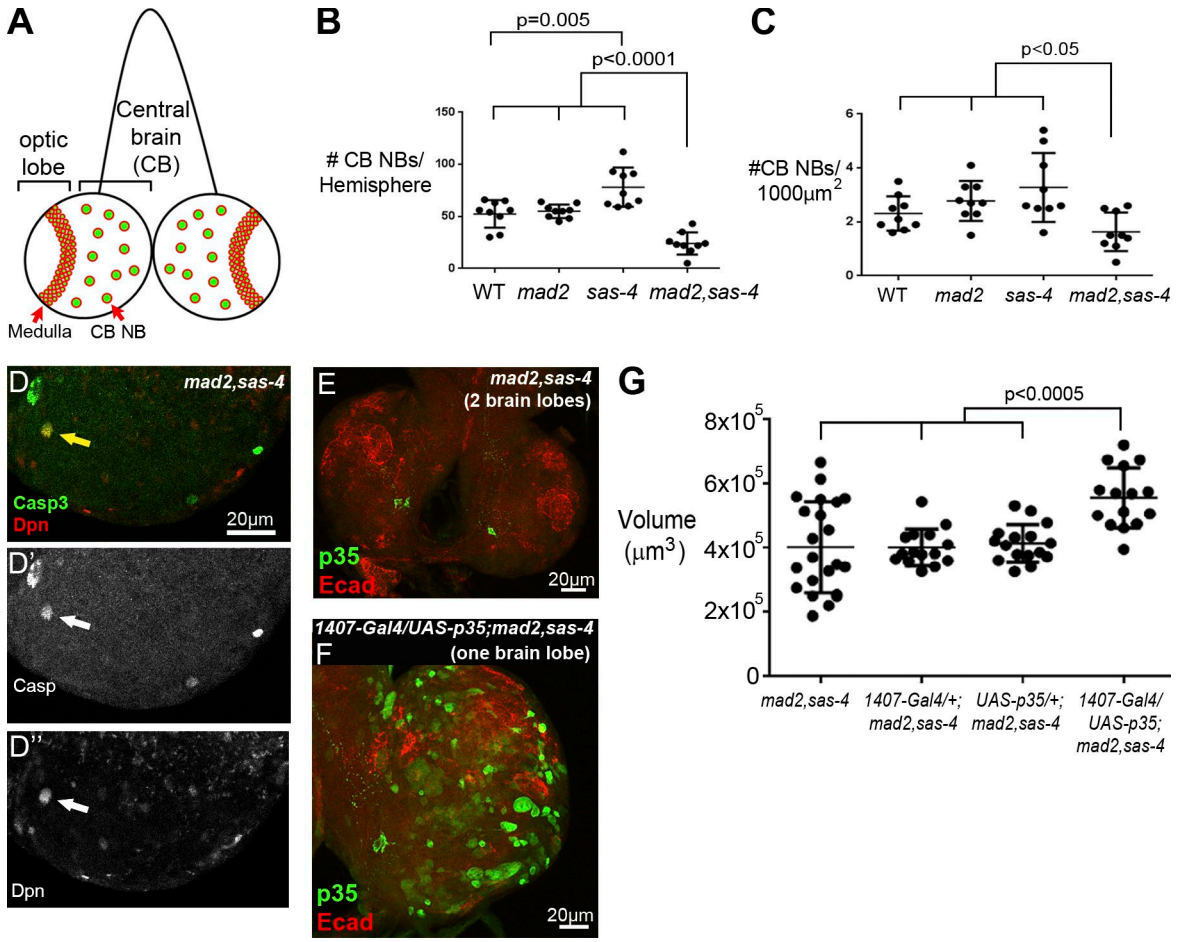


Figure 3. **Cell death caused by centrosome/SAC loss reduces the neural progenitor pool.** (A) Diagram of the third instar brain indicating optic lobes and central brain, as well as the locations of medullary and central brain NBs. (B and C) Double mutant brains possessed significantly fewer NBs per hemisphere (B) or when corrected for smaller brain size (C). (D) Casp3 (green) and the NB marker Dpn (red) indicate that some apoptotic cells were NBs. The arrows in D–D'' highlight a cell that stained positive for both Casp3 and Dpn. D' shows the Casp channel only, revealing dying cells; D'' shows the Dpn channel only, marking NBs. (E) p35 (green) was not expressed in WT brains. Ecad outlines brain morphology. (F) Misexpressing p35 by *1407-Gal4* drove robust p35 expression, particularly in NBs. E and F are maximum-intensity projections. (G) Expressing p35 in *mad2 sas-4* increased brain size. Error bars represent means ± SD.

A and B). Collectively, our data suggest that the reduced brain size and NB number in *mad2 sas-4* brains stem from multiple defects, including NB death and loss of the progeny those NBs should have produced as well as potential defects in NB differentiation and cell cycle reentry.

### Disruption of brain development coincides with increased proliferation

We next defined the developmental basis of the dramatic phenotypes of late third instar double mutants. In WT, the ~100 CB NBs are specified during embryogenesis, but most then pause in the cell cycle. By second instar, those NBs reenter the cell cycle and begin to produce progeny (Homem and Knoblich, 2012), and new optic lobe NBs arise by conversion from neuroepithelial cells and start dividing. Thus, the number of mitotic cells increases as larval development proceeds (compare WT brains at different stages: e.g., Fig. 5 C vs. Fig. 4 A). To determine whether early defects in NB survival or mitotic rate contribute to the defects seen in late third instar double mutants, we examined late embryonic, second instar, and mid–third instar brains. The embryonic central nervous system of WT and *mad2 sas-4* mutants appeared identical (Fig. 5, A and B), though at this stage maternally contributed proteins may suffice (Basto et al., 2006). At second instar, when the mitotic cell number is still low (Fig. 5, C and F), WT and *mad2 sas-4* brains exhibited no differences in brain size, mitotic index, or apoptosis (Fig. 5, C–I). However, by mid–third instar (4 d AEL), when WT proliferation and brain size increase dramatically (Fig. 5, M and O), we observed significantly smaller brains (Fig. 5, M–O) and elevated apoptosis in double mutants (Fig. 5, P–R), suggesting that the death of mitotic NBs and loss of their progeny play contributing roles in limiting the growth that normally occurs in third instars.

We also examined whether defective asymmetric NB division, which maintains NB fate and generates differentiating progeny and thus neurons, contributed to reduced brain size. NB progeny are identifiable by nuclear Pros. However, both second and third instar *mad2 sas-4* CB NBs are capable of multiple rounds of asymmetric division, as there are numerous Pros$^+$ progeny adjacent to CB NBs (Figs. 4, F–H; and 5, J–L; CB NBs in *mad1/Df;sas-4* double mutants also remained associated with Pros$^+$ progeny; Fig. S3, F and G). Live imaging third instar *mad2 sas-4* brains also revealed normal asymmetric divisions (Fig. 4 I and Video 3). Intriguingly, disrupted asymmetric

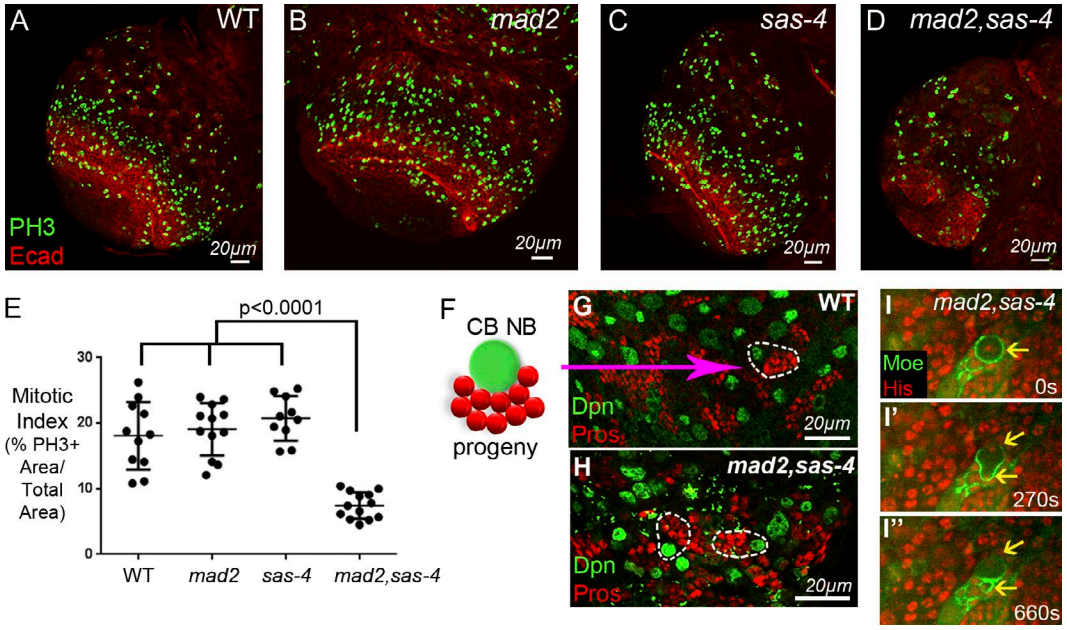


Figure 4. **Centrosome/SAC loss reduces NB proliferation, but asymmetric division still occurs.** (A–E) Mitotic marker PH3. There were significantly fewer dividing cells in *mad2 sas-4* brains, quantified in E. Error bars represent means ± SD. (F) A single CB NB (Dpn$^+$, green) generated several adjacent progeny (Pros$^+$, red). (G and H) Examples of CB NBs (green) and adjacent progeny (red) in WT and *mad2 sas-4*, indicated by the dashed circles. (I) Still images from Video 3 of *mad2 sas-4* expressing Moe:GFP and the chromatin marker His:RFP. Arrows indicate mitotic CB NBs undergoing asymmetric division to maintain the NB (I′) and to produce a smaller daughter bound for differentiation (I′′).

divisions that occur in acentrosomal fly NBs (*sas-4* mutant) result in symmetric division (Basto et al., 2006), in which both daughters retain NB fate, thus increasing NB number (Fig. 3 B) and driving tumor formation (Caussinus and Gonzalez, 2005; Betschinger et al., 2006; Lee et al., 2006). These are opposite to the phenotypes we observed in *mad2 sas-4* double mutants, suggesting that SAC loss might help alleviate the tumorigenic potential of acentrosomal NBs.

One aspect of disrupted brain architecture in late third instar *mad2 sas-4* brains was the lack of optic lobes. To determine the underlying defect, we examined development of the outer optic anlagen (OOA), a neuroepithelium that contributes to optic lobe formation (Ngo et al., 2010). At second instar, WT and *mad2 sas-4* OOA appeared similar (Fig. 5, C and D). However, by mid–third instar, the WT OOA/nascent medulla had increased in size and complexity (Fig. 5 S), whereas in *mad2 sas-4* brains, these were notably retarded (Fig. 5 T). Collectively, our data indicate little difference in CB or optic lobe progenitors in second instar double mutants relative to controls. In contrast, during third instar, when WT cell proliferation increased significantly, *mad2 sas-4* brain organization became highly abnormal, suggesting that defects resulting from combined centrosome–SAC loss (e.g., NB apoptosis or potential cell cycle alterations) likely stem from mitotic errors.

### Combined centrosome and SAC loss elevates genome instability

The mitotic roles of centrosomes and the SAC suggested possible effects on chromosome segregation. Loss of the SAC alone did not lead to statistically significant differences in accurate chromosome segregation, and loss of centrosomes alone led to a subtle but statistically elevated level of aneuploidy. In contrast, codepletion led to extremely high rates of aneuploidy and polyploidy, as assessed by karyotyping (Fig. 6, A–D; Buffin et al., 2007; Rahmani et al., 2009; Caous et al., 2015). Polyploidy was also apparent in *mad2 sas-4* brains as enlarged cells/nuclei, some of which were NBs (Fig. 6 E). Remarkably, some polyploid cells were mitotically active (Fig. 6 F). Because chromosome segregation errors can also lead to DNA damage (Janssen et al., 2011; Crasta et al., 2012), we stained for γ-H2Av, a marker of double-stranded DNA breaks (Madigan et al., 2002). Though neither single mutant differed from WT, *mad2 sas-4* brains had increased DNA damage (Fig. 6, G–K). The γ-H2Av signal did not appear to solely represent the apoptotic cells we observed in *mad2 sas-4* brains, as costaining with Casp3 revealed that only 3.7% of cells with γ-H2Av accumulation were also Casp3 positive (4/108 γ-H2Av$^+$ cells from 11 hemispheres; Fig. S4 H). Similarly, only 7.6% of all apoptotic cells were also γ-H2Av positive (4/53 Casp3$^+$ cells from 11 hemispheres). These data suggest that although DNA damage may contribute to some of the cell death in double mutants, most brain cells can tolerate significant DNA damage without inducing apoptosis. Thus, in neural cells, the SAC helps compensate for inefficient spindle assembly in the absence of centrosomes, and conversely, when the SAC is absent, centrosomes ensure accurate chromosome segregation. However, when both are absent, major defects in chromosome segregation occur.

The contrast with epithelial imaginal discs is pronounced: in wing discs, we could not recover cells mutant for both centrosomes and the SAC, and increased aneuploidy of acentrosomal cells was observed only after blocking apoptosis, suggesting that aneuploid cells die rapidly. In contrast, aneuploid and polyploid cells were frequent in *mad2 sas-4* brains, making up ∼80% of all mitotic cells. This far exceeds the apoptotic rate in those brains, indicating robust tolerance for mitotic errors. Perhaps one relevant difference between aneuploid brains versus wing cells lies in their stress

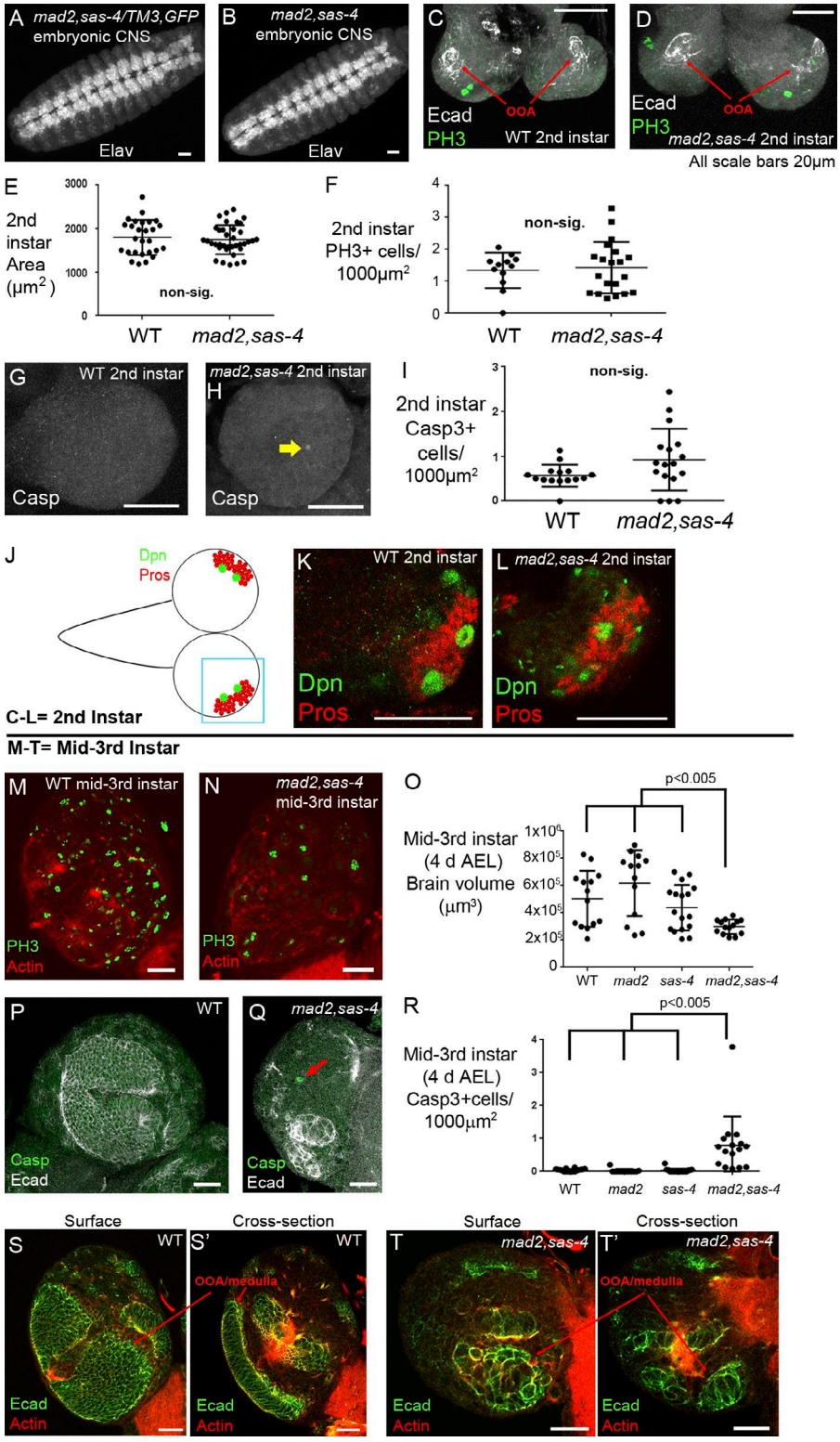


Figure 5. **Significant defects in cell behavior and brain development begin at third instar when mitotic rates increase.** (A and B) Central nervous system (CNS), late-stage WT, and *mad2 sas-4* embryos. Elav marks neurons. (C and D) Little mitosis (PH3+, green) occurred in second instar WT or *mad2 sas-4* brains. The OOA (identified by Ecad expression) was present in both genotypes. (E and F) Brain size (E) and mitotic index (F) at second instar were not altered in *mad2 sas-4*. (G–I) Apoptosis was not increased in second instar *mad2 sas-4* brains. The arrow in H indicates apoptotic cells. (J) Diagram of a few NBs in second instar brains (Dpn+, green) that had already produced clusters of progeny (Pros+, red). (K and L) WT and *mad2 sas-4* NBs and their progeny. (M–O) By mid–third instar, WT and single mutant brains exhibited significant proliferation (PH3+; M) and brain size increases (O). In contrast, *mad2 sas-4* brains began to display reduced size (O) and less proliferation (N). (P–R) *mad2 sas-4* brains exhibited subtle but significant increases in apoptosis (Casp3, green) at mid–third instar. Arrow in Q marks an apoptotic cell. Error bars represent means ± SD. (S) In WT mid–third instar brains, the OOA grew significantly and the medulla emerged (epithelial architecture marked by Ecad, green). (T) The OOA/medulla in *mad2 sas-4* brain also enlarged in mid–third instar but was smaller than WT and lacked normal architecture. S' and T' depict cross-sectional views through the OOA/medulla.

response (Milán et al., 2014). Mitotic errors in wing discs activate JNK signaling, a stress response mediating increased apoptosis in that tissue (Dekanty et al., 2012; Poulton et al., 2014). In *mad2 sas-4* brains, although JNK activity was elevated, misexpressing dominant-negative JNK did not increase brain size (Fig. S4, C–G), unlike blocking apoptosis via p35 misexpression (Fig. 3 G).

## Combined centrosome and SAC loss does not accelerate mitotic timing

Although *mad2 sas-4* wing imaginal disc cells failed to survive (Poulton et al., 2014), our data reveal that many *mad2 sas-4* brain cells survived and proliferated despite high rates of aneuploidy and polyploidy. We thus used live imaging to examine the dynamics and outcomes of NB mitosis in the different mutants.

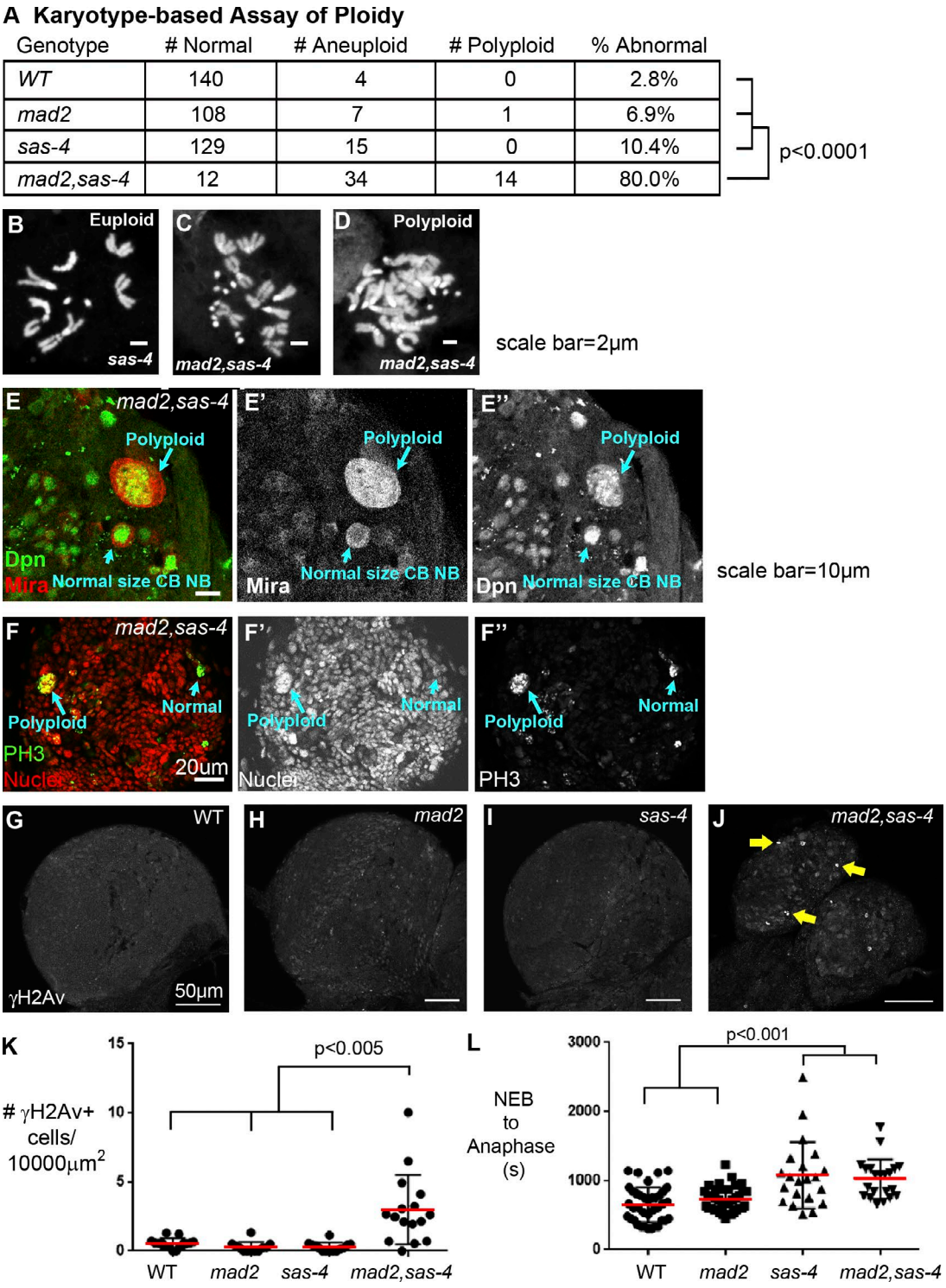


Figure 6. **Loss of centrosomes and the SAC dramatically perturbs genome stability.** (A–D) Karyotype assay. Loss of centrosomes or SAC alone did not dramatically disrupt the accuracy of chromosome segregation, but loss of both elevated aneuploidy and polyploidy. (B–D) Representative euploid or aneuploid/polyploid karyotypes. (E) In *mad2 sas-4* brains, some CB NBs (Dpn+, green; Mira+, red) were normal sized (presumptive diploid or mildly aneuploid), whereas others were abnormally large (presumptive polyploid). E′ shows the Mira channel only, representing the cytoplasmic area of NBs; E′′ shows the Dpn channel only, showing labeling of NB nuclei. (F) Some abnormally large presumed polyploid cells in *mad2 sas-4* brains appeared to be in mitosis (arrows; PH3+, green; nuclei labeled by His:RFP); a normal-sized mitotic cell is also visible. F′ shows the His:RFP channel marking all nuclei; F′′ shows how PH3 staining labels on mitotic cells. (G–K) WT and single mutants did not display high levels of γ-H2Av, whereas *mad2 sas-4* brains contained γ-H2Av+ cells. Arrows in J label cells with high levels of DNA damage. (L) *sas-4* single mutant and *mad2 sas-4* double mutants prolonged the time from NEB to anaphase. Error bars represent means ± SD.

Impressively, the vast majority of mitotic cells in *mad2 sas-4* brains completed cell division. Of 21 *mad2 sas-4* divisions imaged, we noted only two incidents of pronounced mitotic failure: one multipolar division and one failure to complete anaphase (Fig. S5, A–E; and Videos 4 and 5), which may serve as a route to polyploidy. These defects were not observed in live imaging WT or single mutants ($n \geq 21$).

To measure mitotic timing, we analyzed the time from nuclear envelope breakdown (NEB) to anaphase. In contrast to the slight acceleration that was observed in *Drosophila* S2 cells (Orr et al., 2007) and in a previous analysis of NBs (in which time to anaphase was accelerated from 9.7 min to 7.3 min; Buffin et al., 2007), in our experiments, *mad2* loss did not significantly affect mitotic timing in CB NBs (Fig. 6 L). This small discrepancy may reflect different methods of measuring NEB. In contrast, centrosome loss significantly increased the time to anaphase (Fig. 6 L). Surprisingly, *mad2 sas-4* brain cells also took significantly longer than WT or *mad2* single mutants, on par with *sas-4* single mutants (Fig. 6 L). One possible explanation is that degradation of mitotic cyclins is less efficient in acentrosomal cells; previous studies suggest that centrosomes facilitate cyclin B degradation (Huang and Raff, 1999; Wakefield et al., 2000). Inefficient degradation of mitotic cyclins in acentrosomal cells could inhibit anaphase-promoting complex/cyclosome activation and delay anaphase onset independent of the SAC (Caous et al., 2015; Yuan and O'Farrell, 2015). Indeed, NBs mutant for *AuroraA*, which delays cyclin B degradation and anaphase onset, also continue to display delayed anaphase when *mad2* is codepleted (Caous et al., 2015). Alternatively, in *mad2 sas-4* brains, although the SAC is no longer present to regulate anaphase onset, the inefficiency of spindle assembly in acentrosomal cells may be so great that *mad2 sas-4* brain cells cannot physically begin to segregate chromosomes in a timely fashion. Although it is possible that fly Mad2 may have additional functions in spindle assembly (such as MT–kinetochore attachment) like BubR1 (Lampson and Kapoor, 2005) or human Mad2 (Kabeche and Compton, 2012) has, our data from *mad1 sas-4* double mutants suggest that the defects we see are caused by disruptions of the SAC and not by the SAC-independent roles of Mad2.

The importance of centrosomes in mitosis is controversial. One reason for the controversy may be that different cell types respond differently to centrosome loss, with compensatory and surveillance mechanisms having differing efficiencies or sensitivities. For example, although wing disc epithelia exhibit high rates of apoptosis in the absence of centrosomes, NBs at the same developmental stage do not. Our data reveal one mechanism, the SAC, which allows brain cells to tolerate centrosome loss and maintain largely normal mitotic behavior, development, and organismal viability. In contrast, when brains are challenged by a loss of both centrosomes and the SAC, this does trigger elevated apoptosis. This may be a direct result of the aneuploidy and DNA damage we observe, or the mitotic delay that remains in the double mutant cells may somehow become sufficient to induce cell death when the SAC is gone. Furthermore, although aneuploid wing cells undergo apoptosis (Dekanty et al., 2012; Shaukat et al., 2012; Poulton et al., 2014), our study reinforces earlier data demonstrating that many aneuploid/polyploid brain cells survive, and some continue through the cell cycle (e.g., Ripoll et al., 1985; Sunkel and Glover, 1988; Gatti and Baker, 1989; Castellanos et al., 2008). It will be important to evaluate why and how different cell types either tolerate aneuploidy or trigger apoptosis. One hypothesis is that although imaginal discs contain thousands of equivalent progenitors and can regenerate after cell loss by compensatory proliferation, each CB NB produces a unique set of neural progeny (Urbach and Technau, 2003), making replacing apoptotic cells by compensatory proliferation infeasible. This could lead to selection for tolerance of aneuploidy in the brain. Future research will help identify the mechanistic basis for the differential response to mitotic error between these cell types. One difference we found is that although JNK signaling mediates apoptosis caused by mitotic error in wing discs (Dekanty et al., 2012; Poulton et al., 2014), in brain cells, although JNK is elevated, it does not appear essential for cell death. Differences in expression levels of apoptotic regulators may determine the propensity for some cells to initiate apoptosis in response to aneuploidy, as seen in other contexts (Bertet et al., 2014; Fan and Bergmann, 2014). It will be important to determine whether similar or other mechanisms contribute to the differential propensity for apoptosis after mitotic error in brain versus wing disc cells. It also will be of interest to explore whether effects similar to those we observe in fly brains deprived of both centrosomes and the SAC help explain the reduced brain size phenotype seen in mammalian microcephaly.

## Materials and methods

### Fly stocks and husbandry

The following stocks were obtained from the Bloomington Drosophila Stock Center: *yw* (used as the WT in this study; 1495), *HistoneH2Av :RFP* (23651), *sas-4$^{s2214}$* (12119), *1407-Gal4* (=*insc-Gal4*; 8751), *UAS-p35* (5072), *cnn$^{HK21}$* (5039), *Df(3L)BSC438* (24942), *UAS-bsk$^{DN}$* (6409), *UAS-p53$^{H159N}$* (8420), and *Df(2R)w45-30n cn$^{1}$* (deletes *mad1*; 4966). Additional fly stocks used were *mad2$^{P}$* (Buffin et al., 2007), *mad1$^{1}$* (from R. Karess [Emre et al., 2011] via D. Fox [Stormo and Fox, 2016]), *asl$^{mecD}$* (Blachon et al., 2008), *MoesinFABD:GFP* (a gift from D. Kiehart, Duke University, Durham, NC), *TRE-GFP* (Chatterjee and Bohmann, 2012), *BubR1:GFP* (Buffin et al., 2005), and *Hid>GFP* (Tanaka-Matakatsu et al., 2009). Mutant genotypes were balanced by *TM6b Tb Hu* stock, which allowed selection of non-*Tb* homozygous third instar larvae by body shape. When third chromosome mutations were in combination with second chromosome mutations or transgenes, a fused *Cyo:TM6b* balancer was used. Homozygous embryos and second instar larvae were selected using *TM3,Ser,act-GFP*, allowing selection against GFP. All stocks and crosses were maintained at 25°C. Late third instar larvae were collected 6 d AEL, mid–third instar larvae were collected 4 d AEL, and second instar larvae were collected 2 d AEL.

### Immunocytochemistry

Antibody staining was performed as described previously (Roberts et al., 2012). For larval brains, carcasses were inverted to allow penetration to interior tissues. After antibody staining and washing, brains were dissected from the carcass and mounted. Images were captured on LSM Pascal or 880 confocal microscopes (ZEISS). Photoshop CS4 (Adobe) was used to adjust levels so the range of signals spanned the entire output grayscale and to adjust brightness and contrast. Live videos were acquired on a microscope (TE2000-E; Nikon) with a multipoint array scanner (VT-Hawk; VisiTech) with a 40× objective (Nikon), a Ludl emission filter wheel with Semrock filters, and an ORCA-R2 camera (Hamamatsu Photonics). Sample preparation for live imaging was conducted as previously described (Poulton et al., 2014). Videos were processed using ImageJ (National Institutes of Health). The following antibodies and stains were used: α-tubulin (1:2,000; T6199; Sigma-Aldrich), cleaved Casp3 (1:100; 9661S; Cell Signaling

Technology), phosphohistone H3 (1:2,000; 09-797; EMD Millipore), γ-H2Av (1:2,000; a gift from J. Sekelsky, University of North Carolina, Chapel Hill, Chapel Hill, NC), p35 (1:200; 56153; Novus Biologicals), phalloidin (1:500; Molecular Probes), Dpn (1:1,000, a gift from C. Homem and J. Knoblich, Institute of Molecular Biology, Vienna, Austria), Mira (1:1,000, a gift from C. Gonzalez, Institute for Research in Biomedicine, Barcelona, Spain), and Dcp-1 (1:100; 9578S; Cell Signaling Technology). From the Developmental Studies Hybridoma Bank, we obtained Pros (1:10; clone MR1A), Elav (1:10; clone 7E8A10), FasII (1:20; clone 34B3), and Ecad (1:100; clone DCAD2).

### Quantification and statistical analyses

In general, we used two approaches for quantifying the expression levels of various protein markers. To quantitate markers that either expressed in too many cells to feasibly score manually or were too diffuse or overlapping to reliably delineate individual cells, we generated maximum-intensity projections of entire brain z stacks (taken at 1-µm z-depth intervals) and then used ImageJ to threshold the image. We then created a mask of all pixels over the threshold and measured the total area of positive pixels. This was then divided by the total area of that brain, measured by the outline of a ubiquitously expressed marker (e.g., actin) from the same maximum projection. Images from different genotypes were acquired using the same microscope settings, and the same ImageJ threshold was applied to all images across all genotypes. This approach was used to measure markers such as PH3 (in third instar larvae), Dcp-1, and Hid>GFP. The second approach was used to count more readily identifiable individual cells that expressed the marker of interest. In these analyses, expression of the marker of interest was scored at the level of individual cells, analyzing each slice of the entire brain z stack or as a maximum projection. The total number of marker-positive cells was then divided by the volume or area of the brain, again using a ubiquitously expressed marker. This approach was used to quantify Casp3, γ-H2Av, and PH3 (in second instar larvae). For either approach, we then used the Student's *t* test (Excel; Microsoft) to test for statistically significant differences among indicated genotypes.

To karyotype brain cells, we performed chromosome squashes based on a published protocol (Morais da Silva et al., 2013). To statistically compare the incidents of normal versus abnormal karyotypes across genotypes, we used Fisher's exact test (Prism; GraphPad Software).

Brain volume was calculated by modifying the formula for a cylinder $V = \pi r^2 h$. Because the spherical brains were compressed between the slide and coverslip, they took on a cylindrical shape. Because brains are not perfect spheres, the area was directly measured from the central slice of a given z-stack image. This was then multiplied by the height (h) of the brain (z axis) to estimate volume.

Counting of NBs was performed by costaining for Dpn and Mira. We created z-stack images ∼5–7 µm deep into the outer surface of one side of the brain and cropped out the CB region. We then manually counted all cells that expressed both Dpn and Mira and had a minimum cell diameter of 9 µm along their long axes. To standardize for brain size, the number of NBs was then divided by the area of the CB region analyzed. Because *mad2 sas-4* brains lack a clear CB region, we analyzed the entire side of those brains (i.e., we did not crop out a CB region). Although this potentially may have led to scoring of non-CB NBs in *mad2 sas-4* brains (though the vast majority of non-CB NBs would not have reached our size threshold of 9 µm in diameter), their inclusion would have the effect of increasing our estimate of NB numbers in *mad2 sas-4* brains, meaning our conclusion of fewer NBs in *mad2 sas-4* would actually be underestimated based on this analysis. Thus, this approach was a conservative way to estimate the reduction in the CB NB population present in *mad2 sas-4* brains.

### Online supplemental material

Fig. S1 shows the increased apoptosis and reduced brain size in multiple genotypes eliminating centrosomes and the SAC. Fig. S2 shows a further analysis of brain architecture in single and double mutants. Fig. S3 shows how *mad1 sas-4* double mutants phenocopy the *mad2 sas-4* brain development defects. Fig. S4 shows defective differentiation and elevated JNK signaling in *mad2 sas-4* brains. Fig. S5 shows examples of severe mitotic errors in *mad2 sas-4* brains. Video 1 shows that WT brains are highly proliferative. Video 2 shows that *mad2 sas-4* mutant brains have dramatically fewer dividing cells. Video 3 shows how, despite loss of both centrosomes and the SAC, *mad2 sas-4* NBs remain capable of asymmetric division. Video 4 shows failed mitosis in the *mad2 sas-4* mutant brain. Video 5 shows multipolar division in the *mad2 sas-4* brain.


## Acknowledgments

We thank D. Fox, R. Karess, D. Bohmann, T. Avidor-Reiss, J. Sekelsky, C. Homem, J. Knoblich, C. Gonzalez, W. Du, D. Kiehart, the Bloomington Drosophila Stock Center, the Developmental Studies Hybridoma Bank for reagents, T. Perdue for assistance in microscopy, and our University of North Carolina colleagues and the anonymous reviewers for excellent suggestions.

This work was supported by the National Institutes of Health grants R01 GM067236 and R35 GM118096 to M. Peifer and startup funds from the University of North Carolina's Department of Medicine to J.S. Poulton.

The authors declare no competing financial interests.

Author contributions: J.S. Poulton and J.C. Cuningham conducted the experiments. J.S. Poulton, J.C. Cuningham, and M. Peifer analyzed the data. J.S. Poulton and M. Peifer prepared the figures and manuscript.

Submitted: 7 July 2016
Revised: 5 January 2017
Accepted: 13 February 2017


## References


Basto, R., J. Lau, T. Vinogradova, A. Gardiol, C.G. Woods, A. Khodjakov, and J.W. Raff. 2006. Flies without centrioles. *Cell.* 125:1375–1386. http://dx.doi.org/10.1016/j.cell.2006.05.025

Bertet, C., X. Li, T. Erclik, M. Cavey, B. Wells, and C. Desplan. 2014. Temporal patterning of neuroblasts controls Notch-mediated cell survival through regulation of Hid or Reaper. *Cell.* 158:1173–1186. http://dx.doi.org/10.1016/j.cell.2014.07.045

Betschinger, J., K. Mechtler, and J.A. Knoblich. 2006. Asymmetric segregation of the tumor suppressor brat regulates self-renewal in *Drosophila* neural stem cells. *Cell.* 124:1241–1253. http://dx.doi.org/10.1016/j.cell.2006.01.038

Blachon, S., J. Gopalakrishnan, Y. Omori, A. Polyanovsky, A. Church, D. Nicastro, J. Malicki, and T. Avidor-Reiss. 2008. Drosophila *asterless* and vertebrate Cep152 are orthologs essential for centriole duplication. *Genetics.* 180:2081–2094. http://dx.doi.org/10.1534/genetics.108.095141

Buffin, E., C. Lefebvre, J. Huang, M.E. Gagou, and R.E. Karess. 2005. Recruitment of Mad2 to the kinetochore requires the Rod/Zw10 complex. *Curr. Biol.* 15:856–861. http://dx.doi.org/10.1016/j.cub.2005.03.052

Buffin, E., D. Emre, and R.E. Karess. 2007. Flies without a spindle checkpoint. *Nat. Cell Biol.* 9:565–572. http://dx.doi.org/10.1038/ncb1570

Cabernard, C., and C.Q. Doe. 2009. Apical/basal spindle orientation is required for neuroblast homeostasis and neuronal differentiation in *Drosophila*. *Dev. Cell.* 17:134–141. http://dx.doi.org/10.1016/j.devcel.2009.06.009

Caous, R., A. Pascal, P. Romé, L. Richard-Parpaillon, R. Karess, and R. Giet. 2015. Spindle assembly checkpoint inactivation fails to suppress neuroblast tumour formation in *aur*A mutant *Drosophila*. *Nat. Commun.* 6:8879. http://dx.doi.org/10.1038/ncomms9879

Castellanos, E., P. Dominguez, and C. Gonzalez. 2008. Centrosome dysfunction in *Drosophila* neural stem cells causes tumors that are not due to genome instability. *Curr. Biol.* 18:1209–1214. http://dx.doi.org/10.1016/j.cub.2008.07.029

Caussinus, E., and C. Gonzalez. 2005. Induction of tumor growth by altered stem-cell asymmetric division in *Drosophila melanogaster*. *Nat. Genet.* 37:1125–1129. http://dx.doi.org/10.1038/ng1632

Chatterjee, N., and D. Bohmann. 2012. A versatile ΦC31 based reporter system for measuring AP-1 and Nrf2 signaling in *Drosophila* and in tissue culture. *PLoS One.* 7:e34063. http://dx.doi.org/10.1371/journal.pone.0034063

Crasta, K., N.J. Ganem, R. Dagher, A.B. Lantermann, E.V. Ivanova, Y. Pan, L. Nezi, A. Protopopov, D. Chowdhury, and D. Pellman. 2012. DNA breaks and chromosome pulverization from errors in mitosis. *Nature.* 482:53–58. http://dx.doi.org/10.1038/nature10802

Dekanty, A., L. Barrio, M. Muzzopappa, H. Auer, and M. Milán. 2012. Aneuploidy-induced delaminating cells drive tumorigenesis in *Drosophila* epithelia. *Proc. Natl. Acad. Sci. USA.* 109:20549–20554. http://dx.doi.org/10.1073/pnas.1206675109

Emre, D., R. Terracol, A. Poncet, Z. Rahmani, and R.E. Karess. 2011. A mitotic role for Mad1 beyond the spindle checkpoint. *J. Cell Sci.* 124:1664–1671. http://dx.doi.org/10.1242/jcs.081216

Fan, Y., and A. Bergmann. 2014. Multiple mechanisms modulate distinct cellular susceptibilities toward apoptosis in the developing *Drosophila* eye. *Dev. Cell.* 30:48–60. http://dx.doi.org/10.1016/j.devcel.2014.05.007

Gatti, M., and B.S. Baker. 1989. Genes controlling essential cell-cycle functions in Drosophila melanogaster. *Genes Dev.* 3:438–453. http://dx.doi.org/10.1101/gad.3.4.438

Genin, A., J. Desir, N. Lambert, M. Biervliet, N. Van Der Aa, G. Pierquin, A. Killian, M. Tosi, M. Urbina, A. Lefort, et al. 2012. Kinetochore KMN network gene $CASC_5$ mutated in primary microcephaly. *Hum. Mol. Genet.* 21:5306–5317. http://dx.doi.org/10.1093/hmg/dds386

Gogendeau, D., K. Siudeja, D. Gambarotto, C. Pennetier, A.J. Bardin, and R. Basto. 2015. Aneuploidy causes premature differentiation of neural and intestinal stem cells. *Nat. Commun.* 6:8894. http://dx.doi.org/10.1038/ncomms9894

Hayden, M.A., K. Akong, and M. Peifer. 2007. Novel roles for APC family members and Wingless/Wnt signaling during *Drosophila* brain development. *Dev. Biol.* 305:358–376. http://dx.doi.org/10.1016/j.ydbio.2007.02.018

Homem, C.C., and J.A. Knoblich. 2012. *Drosophila* neuroblasts: a model for stem cell biology. *Development.* 139:4297–4310. http://dx.doi.org/10.1242/dev.080515

Huang, J., and J.W. Raff. 1999. The disappearance of cyclin B at the end of mitosis is regulated spatially in *Drosophila* cells. *EMBO J.* 18:2184–2195. http://dx.doi.org/10.1093/emboj/18.8.2184

Ito, K., and T. Awasaki. 2008. Clonal unit architecture of the adult fly brain. *Adv. Exp. Med. Biol.* 628:137–158. http://dx.doi.org/10.1007/978-0-387-78261-4_9

Janssen, A., M. van der Burg, K. Szuhai, G.J. Kops, and R.H. Medema. 2011. Chromosome segregation errors as a cause of DNA damage and structural chromosome aberrations. *Science.* 333:1895–1898. http://dx.doi.org/10.1126/science.1210214

Kabeche, L., and D.A. Compton. 2012. Checkpoint-independent stabilization of kinetochore-microtubule attachments by Mad2 in human cells. *Curr. Biol.* 22:638–644. http://dx.doi.org/10.1016/j.cub.2012.02.030

Klingseisen, A., and A.P. Jackson. 2011. Mechanisms and pathways of growth failure in primordial dwarfism. *Genes Dev.* 25:2011–2024. http://dx.doi.org/10.1101/gad.169037

Lampson, M.A., and T.M. Kapoor. 2005. The human mitotic checkpoint protein BubR1 regulates chromosome–spindle attachments. *Nat. Cell Biol.* 7:93–98. http://dx.doi.org/10.1038/ncb1208

Lee, C.Y., K.J. Robinson, and C.Q. Doe. 2006. Lgl, Pins and aPKC regulate neuroblast self-renewal versus differentiation. *Nature.* 439:594–598. http://dx.doi.org/10.1038/nature04299

Lerit, D.A., and J.S. Poulton. 2016. Centrosomes are multifunctional regulators of genome stability. *Chromosome Res.* 24:5–17. http://dx.doi.org/10.1007/s10577-015-9506-4

Madigan, J.P., H.L. Chotkowski, and R.L. Glaser. 2002. DNA double-strand break-induced phosphorylation of *Drosophila* histone variant H2Av helps prevent radiation-induced apoptosis. *Nucleic Acids Res.* 30:3698–3705. http://dx.doi.org/10.1093/nar/gkf496

Megraw, T.L., J.T. Sharkey, and R.S. Nowakowski. 2011. Cdk5rap2 exposes the centrosomal root of microcephaly syndromes. *Trends Cell Biol.* 21:470–480. http://dx.doi.org/10.1016/j.tcb.2011.04.007

Milán, M., M. Clemente-Ruiz, A. Dekanty, and M. Muzzopappa. 2014. Aneuploidy and tumorigenesis in *Drosophila*. *Semin. Cell Dev. Biol.* 28:110–115. http://dx.doi.org/10.1016/j.semcdb.2014.03.014

Mirzaa, G.M., B. Vitre, G. Carpenter, I. Abramowicz, J.G. Gleeson, A.R. Paciorkowski, D.W. Cleveland, W.B. Dobyns, and M. O'Driscoll. 2014. Mutations in CENPE define a novel kinetochore-centromeric mechanism for microcephalic primordial dwarfism. *Hum. Genet.* 133:1023–1039. http://dx.doi.org/10.1007/s00439-014-1443-3

Morais da Silva, S., T. Moutinho-Santos, and C.E. Sunkel. 2013. A tumor suppressor role of the Bub3 spindle checkpoint protein after apoptosis inhibition. *J. Cell Biol.* 201:385–393. http://dx.doi.org/10.1083/jcb.201210018

Musacchio, A. 2015. The molecular biology of spindle assembly checkpoint signaling dynamics. *Curr. Biol.* 25:R1002–R1018 (published erratum appears in *Curr. Biol.* 2015. 25:3017). http://dx.doi.org/10.1016/j.cub.2015.08.051

Ngo, K.T., J. Wang, M. Junker, S. Kriz, G. Vo, B. Asem, J.M. Olson, U. Banerjee, and V. Hartenstein. 2010. Concomitant requirement for Notch and Jak/Stat signaling during neuro-epithelial differentiation in the *Drosophila* optic lobe. *Dev. Biol.* 346:284–295. http://dx.doi.org/10.1016/j.ydbio.2010.07.036

Nigg, E.A., L. Čajánek, and C. Arquint. 2014. The centrosome duplication cycle in health and disease. *FEBS Lett.* 588:2366–2372. http://dx.doi.org/10.1016/j.febslet.2014.06.030

Orr, B., H. Bousbaa, and C.E. Sunkel. 2007. Mad2-independent spindle assembly checkpoint activation and controlled metaphase–anaphase transition in *Drosophila* S2 cells. *Mol. Biol. Cell.* 18:850–863. http://dx.doi.org/10.1091/mbc.E06-07-0587

Poulton, J.S., J.C. Cuningham, and M. Peifer. 2014. Acentrosomal *Drosophila* epithelial cells exhibit abnormal cell division, leading to cell death and compensatory proliferation. *Dev. Cell.* 30:731–745. http://dx.doi.org/10.1016/j.devcel.2014.08.007

Rahmani, Z., M.E. Gagou, C. Lefebvre, D. Emre, and R.E. Karess. 2009. Separating the spindle, checkpoint, and timer functions of BubR1. *J. Cell Biol.* 187:597–605. http://dx.doi.org/10.1083/jcb.200905026

Ripoll, P., S. Pimpinelli, M.M. Valdivia, and J. Avila. 1985. A cell division mutant of drosophila with a functionally abnormal spindle. *Cell.* 41:907–912. http://dx.doi.org/10.1016/S0092-8674(85)80071-4

Roberts, D.M., M.I. Pronobis, K.M. Alexandre, G.C. Rogers, J.S. Poulton, D.E. Schneider, K.C. Jung, D.J. McKay, and M. Peifer. 2012. Defining components of the ßcatenin destruction complex and exploring its regulation and mechanisms of action during development. *PLoS One.* 7:e31284. http://dx.doi.org/10.1371/journal.pone.0031284

Rusan, N.M., and M. Peifer. 2007. A role for a novel centrosome cycle in asymmetric cell division. *J. Cell Biol.* 177:13–20. http://dx.doi.org/10.1083/jcb.200612140

Shaukat, Z., H.W. Wong, S. Nicolson, R.B. Saint, and S.L. Gregory. 2012. A screen for selective killing of cells with chromosomal instability induced by a spindle checkpoint defect. *PLoS One.* 7:e47447. http://dx.doi.org/10.1371/journal.pone.0047447

Stormo, B.M., and D.T. Fox. 2016. Distinct responses to reduplicated chromosomes require distinct Mad2 responses. *eLife.* 5:15204. http://dx.doi.org/10.7554/eLife.15204

Sunkel, C.E., and D.M. Glover. 1988. polo, a mitotic mutant of Drosophila displaying abnormal spindle poles. *J. Cell Sci.* 89:25–38.

Tanaka-Matakatsu, M., J. Xu, L. Cheng, and W. Du. 2009. Regulation of apoptosis of *rbf* mutant cells during *Drosophila* development. *Dev. Biol.* 326:347–356. http://dx.doi.org/10.1016/j.ydbio.2008.11.035

Urbach, R., and G.M. Technau. 2003. Molecular markers for identified neuroblasts in the developing brain of *Drosophila*. *Development.* 130:3621–3637. http://dx.doi.org/10.1242/dev.00533

Wakefield, J.G., J.Y. Huang, and J.W. Raff. 2000. Centrosomes have a role in regulating the destruction of cyclin B in early *Drosophila* embryos. *Curr. Biol.* 10:1367–1370. http://dx.doi.org/10.1016/S0960-9822(00)00776-4

Wang, C., S. Li, J. Januschke, F. Rossi, Y. Izumi, G. Garcia-Alvarez, S.S. Gwee, S.B. Soon, H.K. Sidhu, F. Yu, et al. 2011. An ana2/ctp/mud complex regulates spindle orientation in *Drosophila* neuroblasts. *Dev. Cell.* 21:520–533. http://dx.doi.org/10.1016/j.devcel.2011.08.002

Yuan, K., and P.H. O'Farrell. 2015. Cyclin B3 is a mitotic cyclin that promotes the metaphase-anaphase transition. *Curr. Biol.* 25:811–816. http://dx.doi.org/10.1016/j.cub.2015.01.053